Thermodynamic Stability of a Cold-Active α-Amylase from the Antarctic Bacterium *Alteromonas haloplanctis*†

Georges Feller,* Dominique d'Amico, and Charles Gerday

Laboratory of Biochemistry, Institute of Chemistry B6, University of Liège, B-4000 Liège, Belgium

Received November 6, 1998; Revised Manuscript Received January 26, 1999

ABSTRACT: The thermal stability of the cold-active α-amylase (AHA) secreted by the Antarctic bacterium *Alteromonas haloplanctis* has been investigated by intrinsic fluorescence, circular dichroism, and differential scanning calorimetry. It was found that this heat-labile enzyme is the largest known multidomain protein exhibiting a reversible two-state unfolding, as demonstrated by the recovery of ΔH_{cal} values after consecutive calorimetric transitions, a $\Delta H_{cal}/\Delta H_{eff}$ ratio close to unity, and the independence of unfolding thermodynamic parameters of scan rates. By contrast, the mesophilic α-amylases investigated here (from porcine pancreas, human salivary glands, yellow meal beetle, *Bacillus amyloliquefaciens*, and *Bacillus licheniformis*) unfold irreversibly according to a non-two-state mechanism. Unlike mesophilic α-amylases, the melting point of AHA is independent of calcium and chloride binding while the allosteric and structural functions of these ions are conserved. The thermostability of AHA at optimal conditions is characterized by a T_m of 43.7 °C, a ΔH_{cal} of 238 kcal mol^{-1}, and a ΔC_p of 8.47 kcal mol^{-1} K^{-1}. These values were used to calculate the Gibbs free energy of unfolding over a wide range of temperatures. This stability curve shows that (a) the specific ΔG_{max} of AHA [22 cal (mol of residue)$^{-1}$] is 4 times lower than that of mesophilic α-amylases, (b) group hydration plays a crucial role in the enzyme flexibility at low temperatures, (c) the temperature of cold unfolding closely corresponds to the lower limit of bacterial growth, and (d) the recombinant heat-labile enzyme can be expressed in mesophilic hosts at moderate temperatures. It is also argued that the cold-active α-amylase has evolved toward the lowest possible conformational stability of its native state.

Psychrophilic organisms, either microorganisms, algae, invertebrates, or fish, live in permanently cold environments and have the surprising ability to grow efficiently at temperatures close to the freezing point of cellular water. However, nearly all biochemical reactions involved in cell metabolism are strongly temperature dependent: for instance, reaction rates are reduced 30−80-fold when the medium temperature is decreased from 37 to 0 °C. To cope with this strong temperature dependence of the enzyme reaction rates, these extremophiles synthesize heat-labile enzymes possessing a high specific activity and catalytic efficiency at low temperatures (*1*, *2*). Heat-lability has been commonly related to the lack of selective pressure for stable proteins in cold environments, but this classical view has frequently been challenged. It is now believed that the weak stability reflects a more resilient or flexible enzyme structure, ensuring a better accommodation of substrates and enhancing the fast conformational changes required by catalysis (*3*−*7*). We report here a spectroscopic and microcalorimetric study of *Alteromonas haloplanctis* α-amylase (AHA)[1] showing how the thermodynamic stability of this heat-labile enzyme is tailored by adaptation to low temperatures. It is also shown that this enzyme is unexpectedly well suited to folding studies of large proteins.

Alteromonas haloplanctis A23 is a Gram-negative bacterium collected along the Antarctic ice-shell where the water temperature remains stable between −2 °C and 2 °C. It secretes a Cl^-- and Ca^{2+}-dependent α-amylase (49 340 Da) sharing extensive sequence and structural similarity with vertebrate and insect α-amylases (*8*−*10*). Binding of one chloride and one calcium ion induces the allosteric activation of these α-amylases (*11*, *12*), but calcium also strongly stabilizes their conformation (*13*−*15*). Most microbial α-amylases, such as those secreted by *Bacillus* and *Aspergillus* species, only bind Ca^{2+} and display very low sequence identity with Cl^--dependent enzymes but adopt the same fold (*16*, *17*). All are monomers of about 50 kDa and exhibit a central main domain A formed by a $(\beta/\alpha)_8$-barrel, a small β-pleated domain B protruding between β_3 and α_3, and a C-terminal globular domain C consisting of a Greek key motif. *B. amyloliquefaciens* and *B. licheniformis* are mesophilic strains which synthesize heat-stable α-amylases. This

† This work was supported by the European Community in the form of Network Contract ERBCHCT 940521, Concerted Action BIO4-CT95-0017, and Biotech Program BIO4-CT96-0051, by the Ministère de l'Education, de la Recherche et de la Formation, Concerted Action ARC93/98-170, and by the Région Wallone-Direction Générale des Technologies, Convention 1828.

* Corresponding author. Phone: (32) 04/366 33 43. Fax: (32) 04/366 33 64. E-mail: gfeller@ulg.ac.be.

[1] Abbreviations: AHA, *Alteromonas haloplanctis* α-amylase; PPA, porcine pancreatic α-amylase; BAA, *Bacillus amyloliquefaciens* α-amylase; aa, amino acid(s); Mops, 3-(*N*-morpholino)propanesulfonic acid; Mes, 2-(*N*-morpholino)ethanesulfonic acid; DSC, differential scanning calorimetry; ΔH_{cal}, calorimetric enthalpy of unfolding; ΔH_{eff}, effective or van't Hoff enthalpy of unfolding; ΔC_p, heat capacity change of unfolding; ΔG, Gibbs free energy of unfolding; T_m, melting temperature; T_{max}, temperature of maximum heat absorption.

10.1021/bi982650+ CCC: $18.00
Published on Web 03/13/1999

extra-stability has recently been correlated with the occurrence of a calcium−sodium−calcium metal triad in the main Ca^{2+} binding site, bridging domains A and B of these enzymes (*17*). Representatives of both α-amylase groups have been included in this study as mesophilic references.

MATERIALS AND METHODS

Sources. Recombinant AHA was expressed in *Escherichia coli* grown at 18 °C and purified as described (*10*, *18*). The three-dimensional structure, the catalytic constants, and the ion binding parameters of this recombinant enzyme were found to be identical to those of the wild-type α-amylase (*18*, *19*). Porcine pancreatic α-amylase was from Boehringer Mannheim. Human salivary *B. amyloliquefaciens* and *B. licheniformis* α-amylases were from Sigma. *T. molitor* α-amylase (*20*) was a generous gift of Dr. S. Strobel (Max Planck Institut für Biochemie, Planegg-Martinsried, Germany). The following parameters were used for calculation: AHA (49 340.58 Da, 453 aa), PPA (55 375.16 Da, 496 aa), BAA (54 835.61 Da, 483 aa), human salivary α-amylase (55 906.64 Da, 496 aa), *T. molitor* α-amylase (51 273.78 Da, 471 aa), and *B. licheniformis* α-amylase (55 265.37 Da, 483 aa). Unless otherwise stated, the standard buffer ensuring optimal enzyme stability contained 30 mM Mops−NaOH, 50 mM NaCl, 1 mM $CaCl_2$, pH 7.2.

Spectroscopic Techniques. Thermal unfolding of α-amylases was monitored by fluorescence using a Perkin-Elmer LS50 spectrofluorometer at excitation and emission wavelengths of 280 and 350, nm respectively. The absorbance at 280 nm of the samples (∼60 μg/mL) was below 0.1. The sample chamber was purged with nitrogen to prevent condensation on the optical surfaces at temperatures <5 °C. Raw data were normalized using the pre- and posttransition base line slopes as described (*21*).

Circular dichroism spectra were recorded using a Jobin Yvon CD6 spectropolarimeter under constant nitrogen flow. In the far-UV region, spectra were recorded in a 0.2-cm cell at a protein concentrations of ∼0.3 mg/mL; in the near-UV region, a 1.0-cm cell was used for protein concentrations of ∼1 mg/mL. Mops concentration was reduced to 5 mM in the far-UV region and to 10 mM in the near-UV region. Spectra were averaged over five scans and corrected for the buffer signal. Raw data were expressed in terms of the mean residue ellipticity [θ] using the known mature α-amylase sequences for calculation of the mean residue weight. Both spectrometers were interfaced to a Neslab water bath, and temperature was varied at a rate of 60 K h^{-1}.

Differential Scanning Calorimetry. Measurements were performed using a MicroCal MCS-DSC instrument at a scan rate of 60 K h^{-1} and under 2 atm nitrogen pressure. Samples were dialyzed overnight against the appropriate buffer, the latter being used in the reference cell and for buffer base line determination. Protein concentration was determined by the bicinchoninic acid protein assay reagent (Pierce) after dialysis and was ∼3.5 mg/mL except for *T. molitor* α-amylase (0.63 mg/mL) and human salivary α-amylase (1.4 mg/mL). Buffers used were 30 mM Mops between pH 6.6 and 7.8, 30 mM Mes between pH 5.6 an 6.5, and 50 mM sodium acetate between pH 4.75 and 5.5, and contained 50 mM NaCl and 1 mM $CaCl_2$. When required, calcium and chloride removal was carried out by dialysis as described (*10*) except that Mops buffer was used. When the absence of monovalent anions in the medium was required, calcium was added in the form of $CaSO_4$ (*10*). Thermograms of AHA were analyzed according to a single non-two-state transition model in which T_m, ΔH_{cal}, and ΔH_{eff} are fitted independently using the MicroCal Origin software (version 2.9). Deconvolution of the heat capacity function of mesophilic α-amylases was performed using a model for multiple two-state transitions in which $\Delta H_{cal} = \Delta H_{eff}$ for each transition. The magnitude and source of the errors in the T_m and enthalpy values have been discussed elsewhere (*22*). Fitting standard errors on a series of five DSC measurements made under the same conditions in the present study were found to be ±0.1 K on T_m and ±4% on both enthalpies.

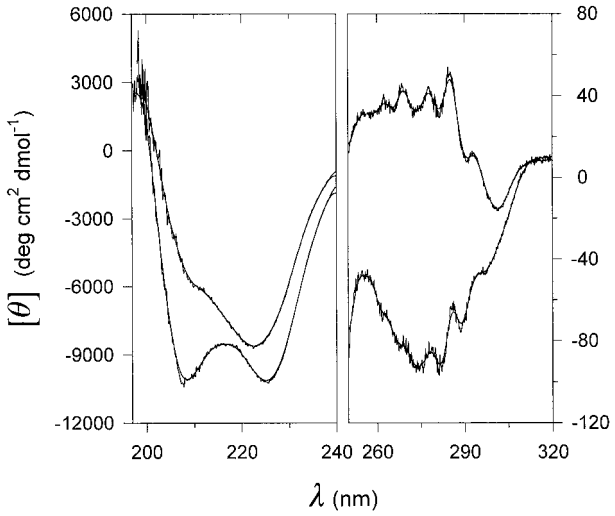

FIGURE 1: Circular dichroism spectra in the far-UV (left panel) and near-UV (right panel) of AHA (upper curves) and PPA (lower curves) at 20 °C. Raw data and smoothed spectra are illustrated. In the far-UV, AHA (0.33 mg/mL) and PPA (0.27 mg/mL) in 5 mM Mops, 50 mM NaCl, 1 mM $CaCl_2$, pH 7.2. In the near-UV, AHA (0.92 mg/mL) and PPA (0.76 mg/mL) in 10 mM Mops, 50 mM NaCl, 1 mM $CaCl_2$, pH 7.2

RESULTS

Circular Dichroism. Crystal structures of AHA (*23*) and of its Cl^-- and Ca^{2+}-dependent α-amylase homologues from vertebrates (*24*−*26*) show an identical α-helix and β-sheet content (30% and 20%, respectively). This, however, is not reflected by the far-UV circular dichroism spectra. Porcine pancreatic α-amylase (PPA), which is the closest structural homologue of AHA, displays the classical spectra of all α-amylases reported so far, with equivalent minima near 208 and 222 nm (Figure 1). Deconvolution of these spectra (*27*) correctly predicts the secondary structure content of the mesophilic α-amylase. By contrast, far-UV spectra of AHA are characterized by a weaker signal at 208 nm, corresponding to an apparent lower α-helix fraction. It appears that in solution, α-helices of AHA possess a weaker optical activity, possibly reflecting less organized helical structures. In the near-UV spectral region, the intensity and sign of AHA spectra reflect the distinctive environment of aromatic residues as already pointed out by crystallographic studies (*19*).

Thermal Stability of α-Amylases. Thermal unfolding recorded in the far- and near-UV shows that both the secondary and tertiary structures of AHA unfold simulta-

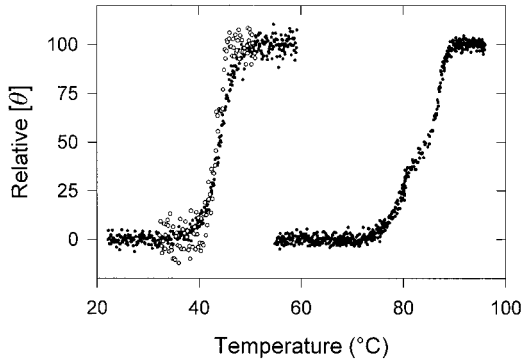

FIGURE 2: Thermal unfolding of AHA (left) and BAA (right) recorded by circular dichroism at 222 nm (●) and 278 nm (○) in 10 mM Mops, 50 mM NaCl, 1 mM $CaCl_2$, pH 7.2. Protein concentrations at 222 nm, AHA (0.30 mg/mL), BAA (0.25 mg/mL); and at 278 nm, AHA (1.45 mg/mL).

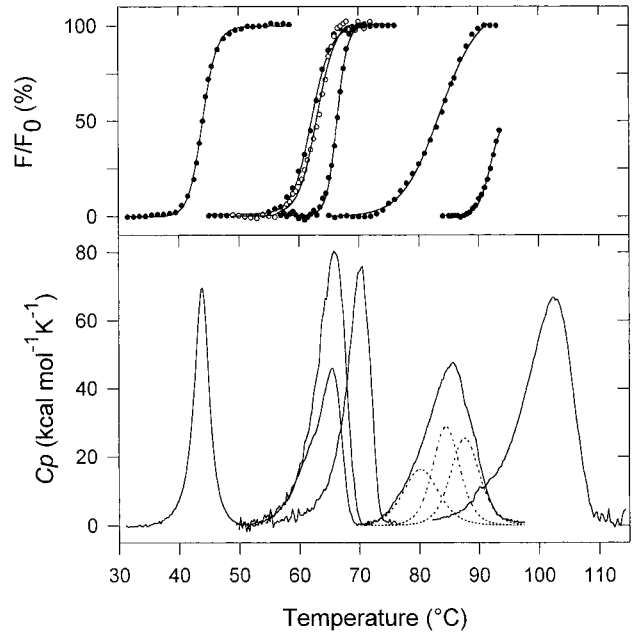

FIGURE 3: Thermal unfolding of α-amylases. Upper panel: relative fluorescence signal. Lower panel: normalized microcalorimetric records. From left to right: AHA, PPA (closed symbols in fluorescence, lower curve in DSC), *T. molitor* α-amylase (open symbols in fluorescence, upper curve in DSC), human salivary α-amylase, BAA (the deconvolution into three cooperative transitions is dashed in DSC), and *B. licheniformis* α-amylase (partial transition in fluorescence normalized on the basis of T_m recorded in DSC). All experiments were performed in 30 mM Mops, 50 mM NaCl, 1 mM $CaCl_2$, pH 7.2. Other conditions are given under Materials and Methods.

neously (Figure 2) with a T_m value estimated at 44 °C. Heat-induced aggregation of mesophilic α-amylases precludes similar reliable analysis, except for *B. amyloliquefaciens* α-amylase (BAA) which displays an intermediate state during secondary structure unfolding (Figure 2). Such an intermediate was also observed during chemically induced unfolding of PPA (*9*) and BAA (not shown). Therefore, these enzymes denature according to a non-two-state process.

Figure 3 illustrates the range of stabilities encountered within the α-amylase family, and Table 1 provides the thermodynamic parameters associated with thermal unfolding recorded by microcalorimetry. As indicated by the large differences in transition temperature T_{max}, the psychrophilic enzyme is by far the least stable when compared to its mesophilic homologues belonging to the Cl^--dependent group or to *Bacillus* and *Aspergillus* α-amylases. A key feature of AHA unfolding is its reversible denaturation according to a single cooperative transition between the native (N) and the unfolded (U) state:

$$N \rightleftharpoons U \qquad (1)$$

By contrast, all mesophilic α-amylases unfold irreversibly as a result of aggregation which cannot be avoided by changing the pH, buffer, or ionic strength or by adding moderate concentrations of urea, guanidinium chloride, pyridine, dimethyl sulfoxide, 2-propanol, EGTA, reducing agents, or detergents. A higher degree of reversibility (~80%) was obtained by guanidinium hydrochloride-induced unfolding (data not shown). On the other hand, these mesophilic α-amylases unfold with a $\Delta H_{cal}/\Delta H_{eff}$ ratio much larger than unity, revealing large deviations from the two-state model, as already suggested by spectroscopic methods. When aggregation does not impair the calorimetric traces, deconvolution of the excess heat capacity function reveals three transitions corresponding to the two-state unfolding of three cooperative units (Figure 3 and Table 1). Similar deconvolutions into three cooperative domains have also been reported for Taka-amylase from *Aspergillus oryzae* (*28*) and for the α-amylase from the hyperthermophilic archaebacterium *Pyrococcus furiosus* (*29*). These three calorimetric units are strongly reminiscent of the three structural domains displayed by their crystal structures, as frequently observed in microcalorimetric analysis of large proteins (*30*).

Equilibrium Unfolding of AHA. The validity of the thermodynamic equations related to eq 1 requires that N and U are in equilibrium and thus that both the reversibility and the two-state transition are unambiguously established. Reversibility is well demonstrated by two consecutive DSC scans of AHA (Figure 4) showing ~99% recovery of ΔH_{cal}, i.e., the calorimetric denaturation enthalpy calculated from the area under the heat absorption peak (*31*). The validity of the two-state model is also demonstrated by a $\Delta H_{cal}/\Delta H_{eff}$ ratio close to unity (*31*) where ΔH_{eff} is measured by the relative amount of the heat absorbed to a given temperature and is equivalent to the van't Hoff enthalpy. As shown in Table 2, AHA fulfills this condition at all pHs from the solubility limit to the optimal pH of stability. Moreover, the independence of the calorimetric traces of AHA of scan rates (between 20 and 120 K h^{-1}) is an additional criterion for the equilibrium unfolding (*32*, *33*) and confirms that no significant kinetically controlled denaturation takes place during calorimetric transitions.

The difference between the heat capacity of the native and the unfolded state (ΔC_p) has been calculated using the Kirchhoff relation:

$$\Delta C_p = \partial \Delta H / \partial T \qquad (2)$$

A plot of ΔH_{cal} as a function of T_m values obtained by changing the pH of the unfolding medium (Figure 5) has a slope of 8.47 ± 0.16 kcal mol^{-1} K^{-1}. This value is in good agreement with those deduced from individual thermogram base lines (Figure 4). The validity of the calculated ΔC_p is further emphasized when this value is replaced in eq 3 along with ΔH_{cal} and T_m recorded in conditions of low stability (pH 5.7). This function predicts a cold unfolding of AHA at

Table 1: Thermodynamic Parameters of α-Amylase Unfolding

α-amylase	T_{max} (°C)	transitions (*n*)	T_m (°C)	ΔH_{cal} (kcal mol^{-1})	$\Sigma\Delta H_{cal}$ (kcal mol^{-1})
Alteromonas haloplanctis	43.7	1	43.7	238	238
porcine pancreas	65.6	2	60.7	122	319[a]
			65.2	197	
Tenebrio molitor (meal beetle)	65.9	3	61.4	101	531
			63.9	183	
			66.4	247	
Aspergillus oryzae (Taka amylase)[b]	69.9	3	64.2	87	488
			67.7	147	
			70.1	254	
human salivary	70.3	2	67.4	144	393[a]
			70.4	249	
Bacillus amyloliquefaciens	85.7	3	79.6	132	487
			84.2	183	
			87.7	172	
Bacillus licheniformis	102.5	3	96.0	165	642
			100.7	233	
			104.3	244	

[a] Minimal value due to aggregation. [b] Data from (*28*).

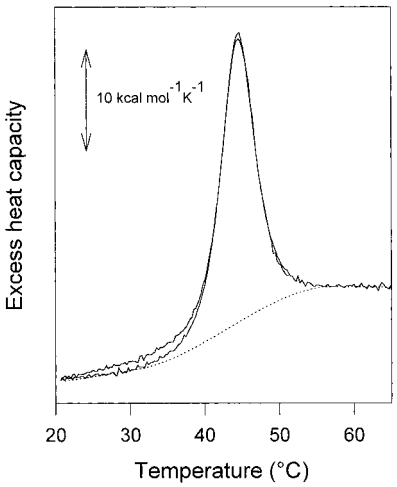

FIGURE 4: Two consecutive DSC endotherms of AHA showing the reversible unfolding of the cold-active enzyme; the progress base line of the reaction is dashed. Rescanning of AHA (3.17 mg/mL) was performed in absence of Ca^{2+} (30 mM Mops, 5 mM EGTA, pH 7.2) in order to minimize posttransition scattering and after in situ cooling at 15 °C for 1 h.

Table 2: Thermodynamic Parameters of AHA Unfolding as a Function of pH

pH	T_m (°C)	ΔH_{cal} (kcal mol^{-1})	ΔH_{eff} (kcal mol^{-1})	$\Delta H_{cal}/\Delta H_{eff}$
5.7	30.6	138	135	1.02
5.8	32.0	139	145	0.96
5.9	34.4	166	175	0.95
6.0	34.7	159	166	0.96
6.1	37.3	179	188	0.95
6.2	37.9	195	210	0.93
6.3	39.1	197	212	0.93
6.4	40.7	223	231	0.97
7.2	43.7	238	224	1.06

+1 °C, and indeed at this pH, both fluorescence and far-UV CD signals recorded at decreasing temperatures display a cold denaturation transition with a midpoint at the corresponding temperature. This is one of the rare favorable cases where ΔC_p can be checked experimentally. The calculated ΔC_p of AHA is among the largest values reported for a protein, but when calculated per mole of residue [18.7 cal (mol of residue)$^{-1}$ K^{-1} for 453 amino acids], the value

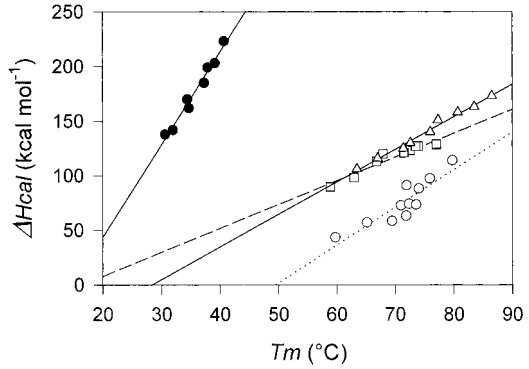

FIGURE 5: Linear dependence of the calorimetric enthalpy on the melting temperature for AHA (●) and the first (○), second (□), and third (△) transitions of BAA.

remains in the usual range for other large proteins [maltose binding protein, $\Delta C_p = 21.3$ cal (mol of residue)$^{-1}$ K^{-1} for 370 amino acids (*34*) or $\Delta C_p = 17.6$ cal (mol of residue)$^{-1}$ K^{-1} (*35*); pepsinogen, $\Delta C_p = 16.5$ cal (mol of residue)$^{-1}$ K^{-1} for 370 amino acids (*36*); subtilisin BPN′, $\Delta C_p = 17.5$ cal (mol of residue)$^{-1}$ K^{-1} for 275 amino acids (*37*)]. The heat capacity change on unfolding of AHA also closely fits with those estimated for the irreversible, non-two-state unfolding of Taka-amylase [8.7 kcal mol^{-1} K^{-1} (*28*)] and of BAA (3.46, 2.17, and 2.98 kcal mol^{-1} K^{-1} for the first, second, and third transitions, respectively) obtained in the present study (Figure 5).

Thermodynamic Stability of AHA. The stability curve of AHA can now be drawn with confidence using the modified Gibbs−Helmholtz equation:

$$\Delta G(T) = \Delta H_m(1 - T/T_m) + \Delta C_p(T - T_m) - T\Delta C_p \ln(T/T_m) \quad (3)$$

Figure 6 displays the denaturation free energy profile of AHA (at pH 7.2) and of small mesophilic and thermophilic proteins (<18 kDa) showing a single cooperative transition as analyzed by the same methodology. The molar Gibbs energy corresponds to the energy required to disrupt the structure, while the specific value (per mole of residue) allows a comparison of proteins with widely different size. The molar ΔG_{max} of AHA is not shifted toward low temperatures but

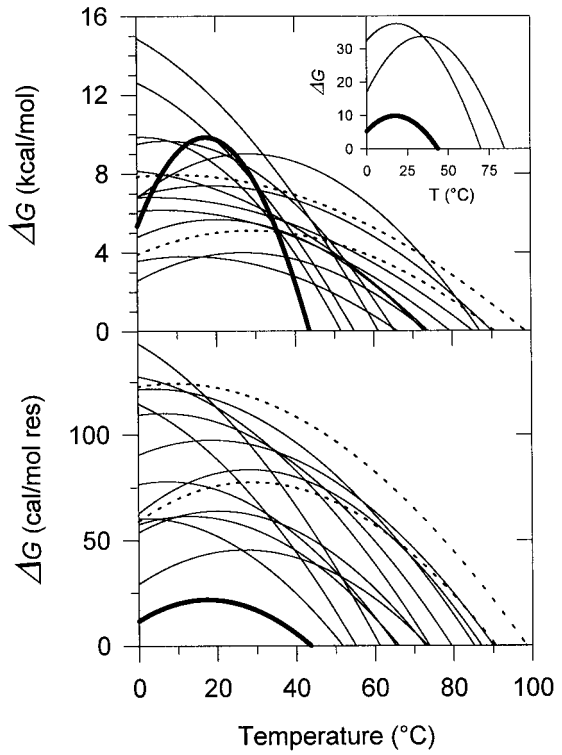

FIGURE 6: Gibbs free energy of denaturation of AHA (heavy line), of mesophilic proteins (continuous lines), and of thermophilic proteins (dashed lines). Upper panel in molar units and lower panel in specific units (per mole of residue). By increasing order of T_m: AHA, T4 lysozyme, barnase, RNase T1, RNase A, spectrin SH3, barstar, phosphocarrier HPr, chymotrypsin inhibitor CI2, protein G IgG binding domain, ovomucoid third domain, thioredoxin, ubiquitin, and the thermophilic proteins Sac7d and Sso7d (*47*, *48*). Inset: molar Gibbs free energy of denaturation of AHA (heavy line), Taka-amylase, and BAA.

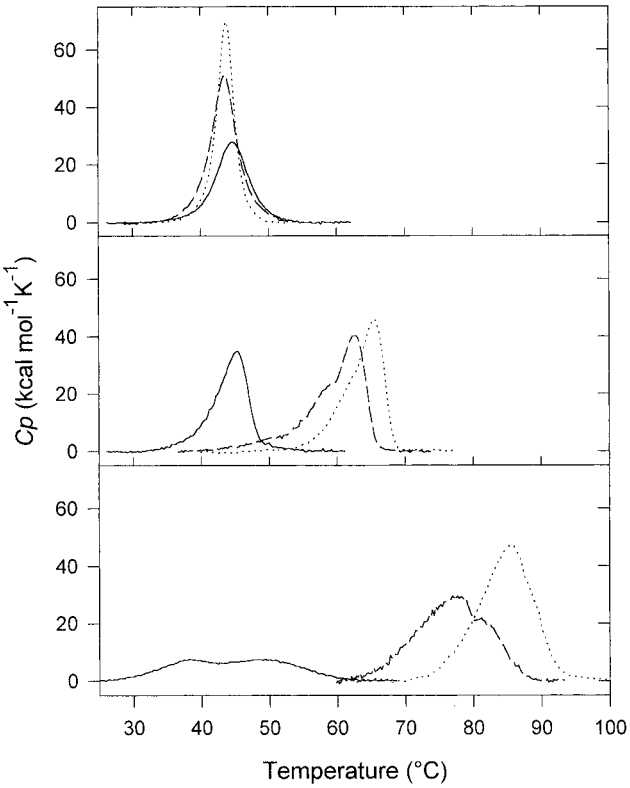

FIGURE 7: Effect of calcium removal on DSC endotherms of AHA (upper panel), PPA (middle panel), and BAA (lower panel). Three conditions are illustrated: the native form with 1 mM Ca^{2+} (dotted); no Ca^{2+} added (dashed); and Ca^{2+} removed (continuous) by 5 mM EGTA (AHA, BAA) or 20 mM EGTA (PPA). All buffers contained 30 mM Mops−NaOH, 50 mM NaCl, pH 7.2, and the indicated concentration of $CaCl_2$ or EGTA. Base line subtracted DSC data have been normalized for protein concentration.

exceeds that of most proteins as a result of the large size of the cold-adapted enzyme. When the specific ΔG is plotted, rather than the molar value, then AHA displays the lowest stability at all temperatures between both T_m's where $\Delta G = 0$. When compared to mesophilic α-amylases (Figure 6, inset), the stability of AHA is 3−4 times lower at all temperatures.

Calcium- and Chloride-Induced Stabilization. Calcium and chloride, when relevant, are integral components of the α-amylase native state and have therefore been included in all the above experiments. In the case of AHA, Ca^{2+} or Cl^- removal drives the $\Delta H_{cal}/\Delta H_{eff}$ ratio from unity in the native state to 1.8 in the ion-free state (by decreasing the ΔH_{eff} term), indicating a less compact structure of the ion-free state (*30*, *35*).

As shown in Figure 7 and Table 3, calcium removal strongly destabilizes mesophilic α-amylases by shifting both T_m and ΔH_{cal} to lower values. Ca^{2+} removal also induces an increased separation of the constitutive transitions (ΔT_m in Table 3), leading to flattened DSC traces. Thermograms of BAA indicate that this enzyme is nearly unfolded when calcium is removed by EGTA. These results demonstrate that calcium is a main determinant of the α-amylase molecule stability: the higher the thermal stability in the native conformation, the higher the Ca^{2+}-induced increase of T_m and of ΔH_{cal}. The behavior of AHA differs significantly, however, because Ca^{2+} removal does not decrease the T_m. On the contrary, the T_m of the Ca^{2+}-loaded form is even slightly lower than that of the apo-enzyme (Table 3). No definitive explanation of this discrepancy can be offered, but the higher T_m of the apo-form can arise from ionic interactions of the carboxylate ligands of the binding site with surrounding residues in the Ca^{2+}-free form. Interestingly also, the T_m values of apo-PPA and apo-BAA are close to that of AHA. It appears, therefore, that the stability of AHA in

Table 3: Effect of Calcium and Chloride Removal on Transition Parameters[a]

α-amylase	condition	ΔT_m (°C)	$\Delta\Delta H_{cal}$ (kcal mol^{-1})	$\Sigma\Delta\Delta H_{cal}$ (kcal mol^{-1})
AHA	no Ca^{2+} [b]	−0.2	−35	−35
	5 mM EGTA	1.0	−62	−62
PPA	no Ca^{2+} [b]	−3.6	−3	−16
		−2.8	−13	
	20 mM EGTA	−19.5	−49	−90
		−20.2	−41	
BAA	no Ca^{2+} [b]	−8.3	−21	−103
		−7.5	−38	
		−6.0	−44	
	5 mM EGTA	−41.6	−67	−321
		−39.3	−149	
		−39.1	−105	
AHA	no Cl^-, 1 mM Ca^{2+}	−0.1	−10	−10
PPA	no Cl^-, 1 mM Ca^{2+}	−4.7	−24	−57
		−4.0	−33	

[a] Data are given as differences (Δ) between the parameters for the native state (Table 1) and the parameters measured in the indicated conditions. [b] No calcium added, ~1 μM Ca^{2+} in buffer estimated by atomic absorption.

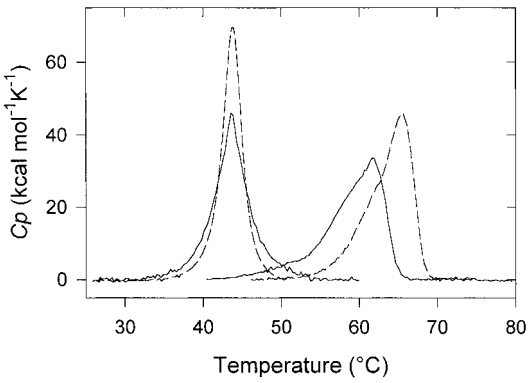

FIGURE 8: Effect of chloride removal on DSC endotherms of AHA (left curves) and PPA (right curves) showing the native enzymes (dotted) and the Cl^--free forms (continuous) obtained after dialysis against 30 mM Mops−NaOH, 1 mM $CaSO_4$, pH 7.2. Base line subtracted DSC data have been normalized for protein concentration.

optimal conditions corresponds to the lowest stability before disruption of the native state of mesophilic α-amylases, as far as T_m values are concerned.

The allosteric activation mediated by the unusual chloride ion is well recognized, but Figure 8 shows that the anion also provides a weak, but noticeable, extra stability to the mesophilic α-amylase. In the case of the psychrophilic enzyme, chloride removal does not alter the T_m value and only slightly decreases ΔH_{cal} (Table 3). In this respect, the effect of chloride on AHA is similar to that of calcium.

DISCUSSION

Despite striking sequence and structure similarity with other α-amylases, it is noteworthy that AHA is the largest known protein that undergoes a reversible equilibrium unfolding. The weak hydrophobicity of its core clusters (*9*, *19*) and the low melting temperature, at which hydrophobic interactions are restrained, certainly account for the reversible character because, unlike mesophilic α-amylases, aggregation does not occur. On the other hand, the unique cooperative unfolding of AHA is best explained by the lack of significant interactions between its structural units and their very weak stability, both leading to the simultaneous denaturation of all the structural elements (shown by circular dichroism) and a merged heat absorption peak. Should these properties be extended to other psychrophilic enzymes, they would obviously constitute an invaluable material for folding studies of large proteins.

Plots of ΔG as a function of temperature give a complete view of the enzyme stability at physiological and nonphysiological temperatures. The low stability of the psychrophilic enzyme [$\Delta G_{max} = 22$ cal (mol of residue)$^{-1}$ at 17 °C and $\Delta G = 12$ cal (mol of residue)$^{-1}$ at 0 °C] essentially arises from the low ΔH_{cal} and T_m values reported in Table 1. They are the obvious consequence of the strongly reduced number of weak interactions stabilizing its three-dimensional structure (*9*, *19*). For comparison, we have estimated the ΔG_{max} of BAA (483 amino acids) to be 70 cal (mol of residue)$^{-1}$ at 34 °C and the ΔG_{max} of Taka-amylase (478 amino acids) to be 79 cal (mol of residue)$^{-1}$ at 12 °C

A striking feature of the AHA stability curve is the fact that unlike mesophilic proteins, the physiological temperature for the psychrophilic enzyme lies far on the left side of the bell-shaped curve (Figure 6). Thus, the main adaptation here is not to drive the thermodynamic stability toward low temperatures but instead to take advantage of the symmetrical ΔG curve to meet the adequate stability. Indeed, at temperatures below that of ΔG_{max}, both the enthalpy and the entropy of denaturation change their sign and become negative. As a result, the enthalpic term changes from a stabilizing factor of the native state to a destabilizing one (*38*). On the right side of the stability curve, mesophilic enzymes reach the necessary balance between the optimal stability (leading to a compact molecule) and flexibility (required for the catalytic function) by using the thermal dissipative force, $-T\Delta S$, which in turn leads to thermal denaturation at high temperatures. By contrast, on the left side, cold denaturation of proteins occurs because the total Gibbs energy of hydration of polar and nonpolar groups is negative and increases in magnitude with decreasing temperatures (*39*). It follows that the potential source of flexibility of the psychrophilic enzyme at 0 °C is radically different from that of mesophiles at 37 °C and mainly arises from group hydration. This finding probably explains the frequently observed low p*I* of psychrophilic enzymes and the improved interactions with the solvent through charged surface residues (*40*−*43*).

There are no substantiated reports of bacterial growth below −12 °C (*44*), and, interestingly, the stability curve in optimal conditions predicts cold unfolding of AHA near −10 °C. Therefore, cold denaturation of proteins such as this α-amylase is certainly one of the limiting factors of life at low temperatures. We have previously shown that the recombinant AHA is not produced in *E. coli* grown at 37 °C whereas it is readily produced at 18 °C while keeping the wild-type kinetic properties (*18*). At 37 °C, the psychrophilic enzyme initiates the thermal unfolding transition (Figure 4) and is either denatured or fails to fold within the *E. coli* cell. By contrast, at 18 °C the stability curve of this enzyme reaches the optimal values (Figure 6), demonstrating the possibility to express heat-labile psychrophilic enzymes in mesophilic hosts at moderate temperatures for biotechnological uses.

Another key feature of AHA conformation is the disappearance of the strong calcium-mediated stabilization recorded for mesophilic α-amylases. Three functions of the main conserved Ca^{2+} ion can be defined: the allosteric activation (*11*, *14*); a structural function by bridging domains A and B, inducing the formation of the substrate-binding site (*17*); and a stabilization role by promoting extra energetically favorable interactions within the protein structure (*45*, *46*). According to our results, Ca^{2+} binding to AHA retains the allosteric function (*9*, *10*) and the structural function (as shown by the increase of ΔH_{cal} and a $\Delta H_{cal}/\Delta H_{eff}$ ratio close to 1 in the Ca^{2+}-loaded form) but has no capacity to provide the usually observed extra-stability, despite Ca^{2+} chelating groups, binding site geometry, and coordination distances identical to those of mesophilic α-amylases (*19*). It seems reasonable to conclude that the low Ca^{2+}-binding constant (*9*) and the lack of stabilization effect arise from the loose conformation of AHA. The same conclusion also applies to chloride binding, although the anion effect is less pronounced. This chloride-induced stabilization can be explained by the bridging of the secondary structures α_D, β_5, and β_8 of the central barrel carrying the chloride ligands.

Noticeably, we were unable up to now to produce site-directed destabilized mutants of AHA: these mutants are denatured a few hours after their production in *E. coli*, unlike stabilized mutants which can be produced in large quantity. This aspect, as well as the disappearance of the ion-mediated extra stability and the simultaneous unfolding of all AHA structural elements, suggests that it has evolved toward a state close to the lowest possible stability, i.e., that the high degree of flexibility required for efficient catalysis at low temperatures precludes further destabilization of the native state. If AHA cannot be less stable (or more resilient), this enzyme should be unable to further adapt to catalysis at low temperature. This limitation would explain the imperfect adaptation of psychrophilic enzymes, i.e., that their activity at low temperature, although very high, remains generally lower than that of mesophilic enzymes at 37 °C.

ACKNOWLEDGMENT

We are grateful to the Institut Français de Recherche et de Technologie Polaire for the support and facilities offered at the Antarctic station Dumont d'Urville during earlier stages of this work. We also thank Dr. S. Strobel (Max Planck Institut für Biochemie, Planegg-Martinsried, Germany) for kindly providing the sample of *T. molitor* α-amylase.

REFERENCES

1. Low, S. P., Bada, J. L., and Somero, G. N. (1973) *Proc. Nat. Acad. Sci. U.S.A. 70*, 430−432.
2. Johnston, I. A., Walesby, N. J., Davison, W., and Goldspink, G. (1975) *Nature 254*, 74−75.
3. Privalov, P. L., Tiktopulo, E. I., and Tischenko, V. M. (1979) *J. Mol. Biol. 127*, 203−216.
4. Hochachka, P. W., and Somero, G. N. (1984) *Biochemical Adaptation*, Princeton University Press, Princeton, NJ.
5. Somero, G. N. (1995) *Annu. Rev. Physiol. 57*, 43−68.
6. Zavodszky, P., Kardos, J., Svingor, A., and Petsko, G. A. (1998) *Proc. Natl. Acad. Sci. U.S.A. 95*, 7406−7411.
7. Fields, P. A., and Somero, G. N. (1998) *Proc. Natl. Acad. Sci. U.S.A. 95*, 11476−11481.
8. Feller, G., Lonhienne, T., Deroanne, C., Libioulle, C., Van Beeumen, J., and Gerday, C. (1992) *J. Biol. Chem. 267*, 5217−5221.
9. Feller, G., Payan, F., Theys, F., Qian, M., Haser, R., and Gerday, C. (1994) *Eur. J. Biochem. 222*, 441−447.
10. Feller, G., le Bussy, O., Houssier, C., and Gerday, C. (1996) *J. Biol. Chem. 271*, 23836−23841.
11. Levitzki, A., and Steer, M. L. (1974) *Eur. J. Biochem. 41*, 171−180.
12. Lifshitz, R., and Levitzki, A. (1976) *Biochemistry 15*, 1987−1993.
13. Violet, M., and Meunier, J. C. (1989) *Biochem. J. 263*, 665−670.
14. Bush, D. S., Sticher, L., van Huystee, R., Wagner, D., and Jones, R. L. (1989) *J. Biol. Chem. 264*, 19392−19398.
15. Boel, E., Brady, L., Brzozowski, A. M., Derewenda, Z., Dodson, G. G., Jensen, V. J., Petersen, S. B., Swift, H., Thim, L., and Woldike, H. F. (1990) *Biochemistry 29*, 6244−6249.
16. Brzozowski, A. M., and Davies, G. D. (1997) *Biochemistry 36*, 10837−10845.
17. Machius, M., Declerck, N., Huber, R., and Wiegand, G. (1998) *Structure 6*, 281−292.
18. Feller, G., le Bussy, O., and Gerday, C. (1998) *Appl. Environ. Microbiol. 64*, 1163−1165.
19. Aghajari, N., Feller, G., Gerday, C., and Haser, R. (1998) *Structure 6*, 1503−1516.
20. Strobl, S., Maskos, K., Betz, M., Wiegand, G., Huber, R., Gomis-Rüth, X., and Glockshuber, R. (1998) *J. Mol. Biol. 278*, 617−628.
21. Pace, C. N. (1986) *Methods Enzymol. 131*, 266−280.
22. Matouschek, A., Matthews, J. M., Johnson, C. M., and Fersht, A. R. (1994) *Protein Eng. 7*, 1089−1095.
23. Aghajari, N., Feller, G., Gerday, C., and Haser, R. (1998) *Protein Sci. 7*, 564−572.
24. Qian, M., Haser, R., and Payan, F. (1993) *J. Mol. Biol. 231*, 785−799.
25. Brayer, G. D., Luo, Y., and Withers, S. G. (1995) *Protein Sci. 4*, 1730−1742.
26. Ramasubbu, N., Paloth, V., Luo, Y., Brayer, G. D., and Levine, M. J. (1996) *Acta Crystallogr. D52*, 435−446.
27. Provencher, S. W., and Glöckner, J. (1981) *Biochemistry 20*, 33−37.
28. Fukada, H., Takahashi, K., and Sturtevant, J. M. (1987) *Biochemistry 26*, 4063−4068.
29. Laderman, K. A., Davis, B. R., Krutzsch, H. C., Lewis, M. S., Griko, Y. V., Privalov, P. L., and Anfinsen, C. B. (1993) *J. Biol. Chem. 268*, 24394−24401.
30. Privalov, P. L. (1982) *Adv. Protein Chem. 35*, 1−104.
31. Privalov, P. L. (1979) *Adv. Protein Chem. 33*, 167−241.
32. Sanchez-Ruiz, J. M., Lopez-Lacomba, J. L., Cortijo, M., and Mateo, P. L. (1988) *Biochemistry 27*, 1648−1652.
33. Lepock, J. M., Ritchie, K. P., Kolios, M. C., Rodahl, A. M., Heinz, K. A., and Kruuv, J. (1992) *Biochemistry 31*, 12706−12712.
34. Ganesh, C., Shah, A. N., Swaminathan, C. P., Surolia, A., and Varadarajan, R. (1997) *Biochemistry 36*, 5020−5028.
35. Novokhatny, V., and Ingham, K. (1997) *Protein Sci. 6*, 141−146.
36. Mateo, P. L., and Privalov, P. L. (1981) *FEBS Lett. 123*, 189−192.
37. Pantoliano, M. W., Whitlow, M., Wood, J. F., Dodd, S. W., Hardman, K. D., Rollence, M. L., and Bryan, P. N. (1989) *Biochemistry 28*, 7205−7213.
38. Privalov, P. L. (1992) in *Protein Folding* (Creighton, T. E., Ed.) pp 83−126, W. H. Freeman and Co., New York.
39. Makhatadze, G. I., and Privalov, P. L.. (1995) *Adv. Protein Chem. 47*, 307−425.
40. Davail, S., Feller, G., Narinx, E., and Gerday, C. (1994) *J. Biol. Chem. 269*, 17448−17453.
41. Genicot, S., Rentier-Delrue, F., Edwards, D., VanBeeumen, J., and Gerday, C. (1996) *Biochim. Biophys. Acta 1298*, 45−57.
42. Feller, G., Zekhnini, Z., Lamotte-Brasseur, J., and Gerday, C. (1997) *Eur. J. Biochem. 244*, 186−191.
43. Russell, R. J. M., Gerike, U., Danson, M. J., Hough, D., and Taylor, G. L. (1998) *Structure 6*, 351−361.
44. Russell, N. J. (1990) *Philos. Trans. R. Soc. London B 326*, 595−611.
45. McPhalen, C. A., Strynadka, N. C. J., and James, M. N. G. (1991) *Adv. Protein Chem. 42*, 77−144.
46. Voordouw, G., Milo, C., and Roche, R. S. (1976) *Biochemistry 15*, 3716−3724.
47. McCrary, B. S., Edmondson, S. P., and Shriver, J. W. (1996) *J. Mol. Biol. 264*, 784−805.
48. Knapp, S., Karshikoff, A., Berndt, K. D., Christova, P., Atanasov, B., and Ladenstein, R. (1996) *J. Mol. Biol. 264*, 1132−1144.

BI982650+